



## Temperature measurements near the contact line of an evaporating meniscus V-groove

Christopher P. Migliaccio, Hemanth K. Dhavaleswarapu, Suresh V. Garimella \*

Cooling Technologies Research Center, School of Mechanical Engineering and Birk Nanotechnology Center, Purdue University, West Lafayette, IN 47907-2088, USA

### ARTICLE INFO

#### Article history:

Received 18 March 2010

Received in revised form 23 October 2010

Accepted 23 October 2010

Available online 17 December 2010

#### Keywords:

Evaporation

Thin liquid film

V-groove

Temperature dip

### ABSTRACT

Evaporation from a meniscus of heptane liquid in a V-groove geometry is experimentally investigated. A thin layer of titanium coated on the backside of the fused quartz groove is electrically heated to provide a constant heat flux. The temperature profile in the evaporating thin film region of the extended meniscus is measured using high-resolution infrared thermography and the temperature suppression in this region is obtained as a function of liquid feeding rate. The meniscus shape is captured using a goniometer. A temperature suppression of  $\sim 0.2$  K in the  $150 \mu\text{m}$  region surrounding the contact line on each side indicates the efficacy of evaporation in the extended meniscus. At a given axial location, the fraction of total meniscus heat transfer which takes place in a  $50 \mu\text{m}$  sub-region measured from the contact line is estimated by an approximate heat balance analysis to be  $\sim 45\%$  for the range of liquid feeding rates explored.

© 2010 Elsevier Ltd. All rights reserved.

### 1. Introduction

In today's high heat flux applications, heat fluxes in excess of  $100 \text{ W/cm}^2$  must often be dissipated from areas on the order of  $1 \text{ cm}^2$ . Cooling technologies that can handle these high fluxes commonly exploit two-phase heat transfer. Heat pipes, thermosyphons, vapor chambers, two-phase cold plates, and capillary pumped loops all rely on evaporation from an extended meniscus to efficiently dissipate large amounts of heat.

A number of researchers have made important contributions to the study of evaporating menisci. The region near the solid–liquid–vapor junction, termed the “thin-film” region, has been of particular interest to researchers due to its exceptional heat transfer characteristics. Deryagin [1] showed that the disjoining pressure gradient due to intermolecular forces in thin liquid films provides the mechanism for replenishment of the liquid lost to evaporation. A detailed development of the equations governing interfacial phenomena, fluid mechanics, and heat transfer of an extended meniscus was presented by Potash and Wayner [2]. Wayner and co-workers [3,4] performed a number of theoretical and experimental investigations in the field. They demonstrated that interferometry is a powerful method for obtaining very high resolution profiles of thin liquid films that can be used in the modeling of interfacial processes.

A number of studies have focused on modeling evaporating thin liquid films in grooves. Holm and Goplen [5] developed an

analytical model of evaporation of liquid in capillary grooves. The region they delineated as the evaporating film region accounted for only 8% of meniscus heat transfer; however, 80% of the total heat transfer was attributed to a thin-film transition region that was located between the evaporating film region and the intrinsic meniscus. Xu and Carey [6] performed experiments with evaporating solvents in V-grooves and developed an analytical model that was in reasonable agreement with their experiment. Their model assumed that all of the heat was dissipated from the extended meniscus. A numerical model developed by Stephan and Busse [7] explored an evaporating meniscus in a V-groove and predicted that approximately 45% of the total heat dissipated by the groove was handled by a microregion of up to  $1 \mu\text{m}$  in thickness. Ma and Peterson [8] developed an experimentally validated model to predict the maximum capillary heat transport capacity of a liquid flowing in V-shaped grooves.

Microparticle image velocimetry ( $\mu\text{PIV}$ ) has been used to investigate fluid velocities near the contact line of evaporating menisci. Dhavaleswarapu et al. [9] and Chamarthy et al. [10] used  $\mu\text{PIV}$  to investigate thermocapillary convection near an evaporating meniscus in capillary tubes. They presented velocity maps in the meniscus that showed strong liquid flow into the thin-film region replenishing liquid lost due to the intense local evaporative heat flux. Flow into the thin-film region of an evaporating sessile droplet was demonstrated by Deegan et al. [11]. They explained that droplets seeded with microparticles tend to leave a ring-shaped deposit after evaporation due to the intense mass transfer occurring near the contact line. More recently,  $\mu\text{PIV}$  was implemented by Dhavaleswarapu et al. [12] to reconstruct velocity fields in evaporating sessile water droplets on a glass substrate. The spatial and temporal distribution

\* Corresponding author. Tel.: +1 765 494 5621.

E-mail address: [sureshg@purdue.edu](mailto:sureshg@purdue.edu) (S.V. Garimella).

### Nomenclature

$f$	example dependent function	$\eta$	fraction of heat flow through the sub-region (%)
$h_{fg}$	latent heat of vaporization (J/kg)	$\theta$	partial derivative of $f$ with respect to an independent quantity
$q$	heat transfer rate (W)	$\sigma$	uncertainty
$q'$	heat transfer rate per unit length (W/m)	$\psi$	liquid feeding rate (kg/s)
$q''$	heat flux (W/m <sup>2</sup> )		
$t$	time (s)		
$T$	temperature (°C)		
$W$	length of the groove in the axial direction ( $\mu\text{m}$ )	<i>Subscripts</i>	
$x$	position on groove wall perpendicular to the axial direction ( $\mu\text{m}$ )	<i>applied</i>	heat applied to groove by joule heating
$x_0$	contact line position ( $\mu\text{m}$ )	<i>dry</i>	non-wetted portion of groove top wall
$y$	axial position in groove measured from edge opposite liquid feeder ( $\mu\text{m}$ )	<i>loss</i>	heat loss from groove
		<i>net</i>	difference between applied and lost heat
		<i>sub-region</i>	heat dissipated through the sub-region of the meniscus
		<i>wet</i>	wetted portion of groove top wall
<i>Greek symbols</i>			
$\delta$	groove wall thickness ( $\mu\text{m}$ )		
$\Delta x$	length of the sub-region ( $\mu\text{m}$ )		

of the local evaporative mass flux was determined, and the temperature distribution in the droplet near the contact line estimated.

Experimental measurement of temperature profiles near the contact line of an evaporating thin film has proven challenging. The use of thermocouples and other temperature-transducing sensors disturbs the liquid–vapor interface. Therefore, other measurement techniques such as thermochromic liquid crystals (TLCs) have been employed [13–15]. TLCs provide very good spatial resolution ( $\sim 1 \mu\text{m}$ ) [13], but suffer from limited life-spans and high measurement uncertainties. Measurement of interfacial temperature with infrared (IR) thermography is an attractive option because of its non-intrusive nature and relatively good resolution. Jiang et al. [16] used infrared imaging to investigate the heat transfer from heated cylinders wetted with liquid. They found that 20–40% of the total meniscus heat transfer was dissipated in an extended meniscus region of length on the order of  $100 \mu\text{m}$ . A temperature drop corresponding to the thin film location was detected by the infrared camera; however, the limits on camera resolution did not allow for an accurate quantitative description of the temperature dip. Buffone and Sefiane [17] investigated thin-film evaporation in capillary tubes using IR imaging on the outer surface of the tube as well as of the liquid meniscus in end view. They observed lower temperatures on the exterior of the tube corresponding to the location of the contact line of the liquid inside, implying that a significant amount of heat was transferred through the thin-film region. More recently, evaporation of an extended meniscus in a channel has been investigated by Dhavale-swarapu et al. [18]. The camera and lens used provided an order-of-magnitude higher spatial resolution ( $\sim 6.3 \mu\text{m}$ ) than past experiments and allowed for the detection of a distinct temperature drop near the contact line of the evaporating liquid.

The present work complements past studies by employing infrared thermography to obtain high spatial resolution ( $\sim 6.3 \mu\text{m}$ ) measurements of the temperature contours near an evaporating liquid meniscus in a groove geometry. A high-end (20 mK temperature sensitivity), science-grade IR camera with a 4X zoom lens is used. A heat balance is used to estimate the efficacy of the heat transfer from a  $50 \mu\text{m}$  long sub-region of the extended meniscus.

## 2. Experimental setup and procedures

A schematic diagram of the test setup is shown in Fig. 1. Due to the working distance of the zoom lens used in this work ( $\sim 13 \text{ mm}$ ), it was not possible to image the inner surface of a V-groove be-

cause of the obstruction posed by the presence of the opposing leg of the V-groove wall. To eliminate this difficulty, the present test setup includes only one half of the groove encompassing just one groove wall and the middle vertical plane; this approach allows for temperature measurements at the contact line to be obtained with no obstruction. The half groove in the test is formed by the intersection of a vertical center wall made from  $150 \mu\text{m}$  thick glass and a groove wall cut from a  $500 \mu\text{m}$  thick fused quartz wafer. The interior angle of the groove measures  $30^\circ (\pm 0.5^\circ)$ , and the center wall rises  $1.58 \text{ mm}$  from the interior apex of the groove. The groove wall extends  $7.10 \text{ mm}$  from the groove apex. The total length of this half groove geometry is  $50 \text{ mm}$ . The groove wall is bonded to the center wall with a bead of solvent-resistant RTV sealant (730, Dow Corning). A  $100 \text{ nm}$  titanium layer is deposited on the backside of the quartz substrate using an e-beam evaporator (SE 600, CHA Industries) at a deposition rate of  $2 \text{ \AA/s}$ . Electrical heating through this layer results in a constant heat flux being applied to the groove wall. To continually replenish liquid lost to evaporation, a syringe pump (PHD 2000, Harvard Apparatus) feeds room-temperature liquid to the groove through a  $150 \mu\text{m}$  inner-diameter capillary tube that is positioned just above the meniscus contact line,  $12.5 \text{ mm}$  from one of the groove edges ( $y = 37.5 \text{ mm}$ ), as shown in Fig. 1. Liquid in the groove forms a meniscus that is pinned at the top of the glass center wall and progressively moves up the quartz wall with increasing feeding rate.

Temperature contours on the groove wall topside (the bare quartz side in contact with the liquid) are recorded with an infrared (IR) camera (Merlin, FLIR Inc.) with a 4X objective ( $2 \text{ mm} \times 1.5 \text{ mm}$  field of view). The IR camera was calibrated with a high-sensitivity, high-stability blackbody (2000 series, SBIR Inc.). The emissivity of the quartz wall was determined in a separate experiment in which half of the bare quartz side of a similarly fabricated quartz wafer section was coated with black paint (Krylon # 1602) of known emissivity 0.96 [19]. The wafer was then heated and a series of images at different wafer temperatures was recorded that included both the painted and bare quartz surfaces. On each side of the interface,  $1000 \mu\text{m} \times 500 \mu\text{m}$  regions of each surface were assumed to be at a uniform temperature, and RTools software (FLIR Inc.) was used to adjust the emissivity of the bare quartz surface until its temperature matched that of the black surface. The emissivity of the quartz surface was found to be 0.715 at  $50^\circ\text{C}$ . Camera calibration and the quartz emissivity determination were performed *in situ* to minimize differences in background radiation.

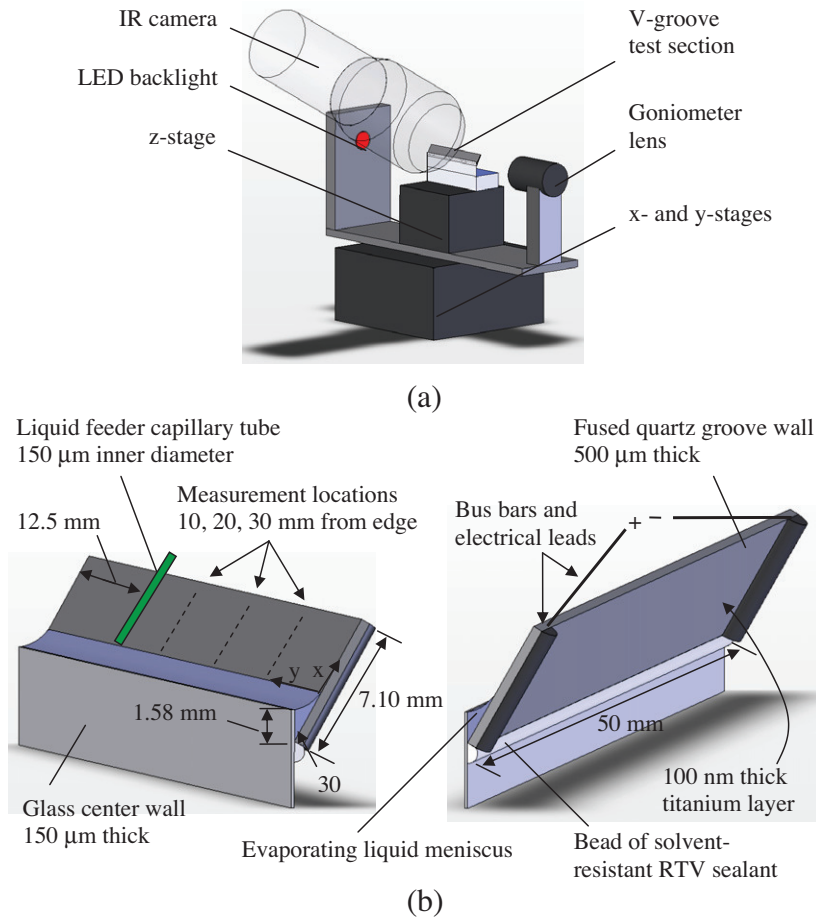


Fig. 1. (a) Perspective view of the test setup. (b) Close-up view of the V-groove test section.

The glass center wall measures 20 mm in total height (although only 1.58 mm of this height is subtended in the half groove), and is attached at its bottom to an acrylic block that is mounted on a set of linear stages that enables precise positioning in the horizontal ( $\pm 5 \mu\text{m}$ ) and vertical directions. Also mounted on the stages is a goniometer (CAM 100, KSV Instruments Ltd.) and backlit LED light that is used to image the meniscus. By mounting the goniometer on the same set of stages as the groove itself, simultaneous imaging of the meniscus shape and the temperature contours is achieved. Meniscus images were obtained at normal ( $10 \mu\text{m}/\text{pixel}$ ) and high magnification ( $2.14 \mu\text{m}/\text{pixel}$ ). The high-magnification images captured approximately 80% of the extent of the meniscus, thus providing high-resolution images in the contact-line region.

The test fluid used is high-purity heptane (Sigma–Aldrich, 99.99%). Heptane was selected as the test fluid because it is highly wetting on quartz and exhibits a very thin liquid film as the contact line is approached. Since a layer of up to  $80 \mu\text{m}$  thick heptane is essentially transparent in the mid-infrared region ( $3\text{--}8 \mu\text{m}$ ) [18], the temperature distribution on the quartz wall beneath the heptane can be measured with the IR camera. For a given set of operational parameters, the system was allowed to operate in excess of 90 min before meniscus profiles or temperature data were recorded, in order to let the system reach a steady state. Experiments were performed in a laboratory environment at standard pressure, an ambient temperature of  $21.5^\circ\text{C}$ , and 29% humidity.

The power input to the system,  $q''_{\text{applied}}$ , is determined from the electrical resistance of the titanium layer and the measured voltage drop across this layer. Uncertainties in the resistance and voltage measurements are  $\pm 0.1 \Omega$  and  $\pm 0.3 \text{ mV}$ , respectively. To determine

the net heat flux to which the wafer is subjected, the heat losses by conduction to the unheated center wall and by convection and radiation to the surroundings are estimated with a dry run of the groove with no liquid present. By progressively varying the power input to the system and measuring the temperature of the quartz wall, a relationship between input power and wall temperature is obtained. This relationship provides a dry-run loss curve for a measured groove wall temperature. During experiments involving the evaporating liquid, the wall temperature far from the liquid region is measured, and is correlated to the dry-run loss curve to estimate the heat losses,  $q''_{\text{loss}}$ , corresponding to that particular wall temperature. The uncertainty in the  $q''_{\text{loss}}$  estimation based on measurement confidence and curve-fitting is  $\pm 3\%$ . The net heat flux,  $q''_{\text{net}}$ , is then found by subtracting  $q''_{\text{loss}}$  from  $q''_{\text{applied}}$ . It was observed that at a given heat input, the temperature of the groove wall far from the evaporating liquid remained essentially constant throughout the tested range of liquid feeding rates; therefore, it is concluded that in this system, the net heat flux to the wafer ( $q''_{\text{net}}$ ) is only dependent on input power ( $q''_{\text{applied}}$ ). Due to the large groove wall area (liquid covers only  $\sim 10\%$  of the total quartz wall area), the heat losses are  $\sim 65\%$  of the total applied power for the results reported here. As a result, changes to the input power on the order of  $\pm 25\%$  change the wall temperature and thus the magnitude of  $q''_{\text{loss}}$ , but leave the net heat flux virtually unchanged. Assuming a liquid temperature rise of  $25^\circ\text{C}$  from the liquid inlet to the thin-film region (which was typical of the tests), the sensible heat gained by the liquid is  $\sim 6\%$  of  $q''_{\text{applied}}$  and therefore neglected in our analysis. As discussed in Section 3.3, this assumption makes little difference in the estimation of meniscus sub-region heat transfer.

### 3. Results and discussion

#### 3.1. Dependence of meniscus shape on feeding rate

The meniscus shape of an evaporating liquid film is determined by the capillary and disjoining pressure gradients; the meniscus shape in turn governs the amount of liquid that is fed to the thin-film region. In this work, images of the meniscus were digitally processed using an edge-detection algorithm in MATLAB [20]. With the overall meniscus length known from the normal-magnification image, the normal- and high-magnification meniscus data were reconciled into one data set which has high resolution over  $\sim 80\%$  of the meniscus length (and most importantly in the evaporating thin film region of the extended meniscus) and lower resolution in the remaining 20% of the intrinsic meniscus. This combined image data set was then fit with a fourth-order polynomial. The uncertainty in the meniscus shape curve fit is  $\pm 1.5 \mu\text{m}$ ; however, this estimate does not include errors in determination of the liquid-vapor interface position associated with the edge detection algorithm. Edge effects at the ends of the groove, while important in the heat transfer analysis, did not affect the meniscus imaging because liquid at the edges ( $\sim 1 \text{ mm}$  in extent in the axial direction) was kept from spilling over the groove edges by surface tension forces. By focusing the goniometer on the liquid at an axial location remote from the groove end, the backlit images recorded the bulk meniscus shape, which was observed to be the same along the length of the groove, except for the end regions and in a  $\sim 500 \mu\text{m}$  region where the liquid was fed to the meniscus. Fig. 2 shows a representative meniscus image with its corresponding polynomial fit superimposed.

As all liquid fed to the meniscus evaporates, the feeding rate is equal to the evaporation rate. The meniscus shape is dependent on the feeding rate and applied heat flux; however, in this work, only changes with feeding rate are explored. Ref. [18] discusses the meniscus shape dependence on applied heat flux for a meniscus in a channel. Fig. 3 shows the meniscus profiles for the feeding rates studied at a net applied heat flux of  $600 \text{ W/m}^2$ . The interfacial area increases with increasing feeding rate as the contact line moves farther up the groove wall. Throughout the range of feeding rates, the apparent contact angle remains fairly constant at  $\sim 22 \pm 1^\circ$ , and the meniscus profiles out to  $200 \mu\text{m}$  from the contact line have virtually the same shape. At a distance of approximately  $175 \mu\text{m}$  from the contact line, the meniscus thickness reaches

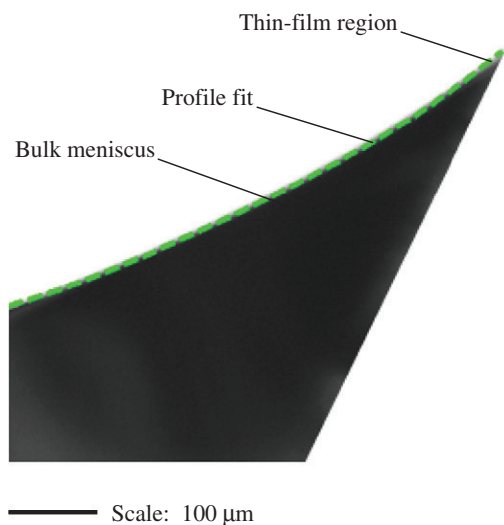


Fig. 2. High-magnification meniscus image with meniscus-profile fit superimposed.

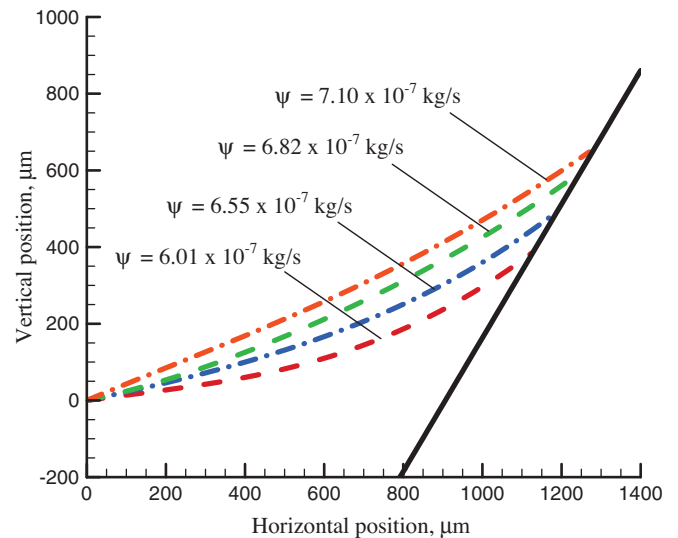


Fig. 3. Meniscus profile dependence on liquid feeding rate at  $q''_{\text{net}} = 600 \text{ W/m}^2$ .

$80 \mu\text{m}$  – a level at which increases in heptane film thickness lead to a sharp decrease in mid-range IR transmissivity [18]. As a result, IR images of the wetted groove wall are only reliable to a distance of up to  $175 \mu\text{m}$  from the contact line.

#### 3.2. Microscale temperature measurements

Infrared temperature images of the extended meniscus region were obtained at three axial locations along the groove:  $y = 10, 20,$  and  $30 \text{ mm}$ . To ensure that the temperature distribution measured is indeed that of the wetted quartz wall (and not of the heptane layer), the region of interest defined in this work is restricted to  $150 \mu\text{m}$  on each side of the contact line. As discussed earlier, the heptane layer thickness over this extent of the meniscus is less than  $80 \mu\text{m}$ , and therefore remains essentially transparent in the mid-IR range. Fig. 4 presents a representative IR image with a dashed line to indicate the region of interest for the thermal analysis. The analysis was performed with the assumption that the evaporation rate of heptane from the meniscus at any axial location along the groove was constant.

Time- and area-averaged temperature profiles of the quartz groove wall extending over a region  $150 \mu\text{m}$  from the contact line on either side are presented for a fixed measurement location ( $y = 10 \text{ mm}$ ) and at different feeding rates in Fig. 5; similar profiles for a constant feeding rate of  $\psi = 6.55 \times 10^{-7} \text{ kg/s}$  but at three different axial measurement locations are shown in Fig. 6. Solid lines represent the curve-fitted temperature, while measurement uncertainties due to thermal noise and time- and area-averaging are represented by the dashed-line envelopes ( $\pm 0.16 \text{ K}$ ). The profiles shown in the figure are measured at a net heat flux of  $600 \text{ W/m}^2$  and a range of feeding rates. Position along the groove wall is depicted on the  $x$ -axis, with 0 representing the contact line location, and  $-x$  and  $+x$  representing the wetted and non-wetted regions, respectively. The experimental setup did not allow for IR imaging of the heater surface on the back side of the groove. Hence, unlike in Ref. [18], where temperature profiles on both top and bottom sides of the wafer were averaged to obtain a mean temperature for analysis, in this work only the wafer top temperature profiles are considered.

The location of the contact line is taken to be the minimum temperature point in the profiles, and a temperature drop of  $\sim 0.2 \text{ K}$  is seen in the  $300 \mu\text{m}$  region that extends  $150 \mu\text{m}$  from the contact line in both directions. This is comparable to the dips

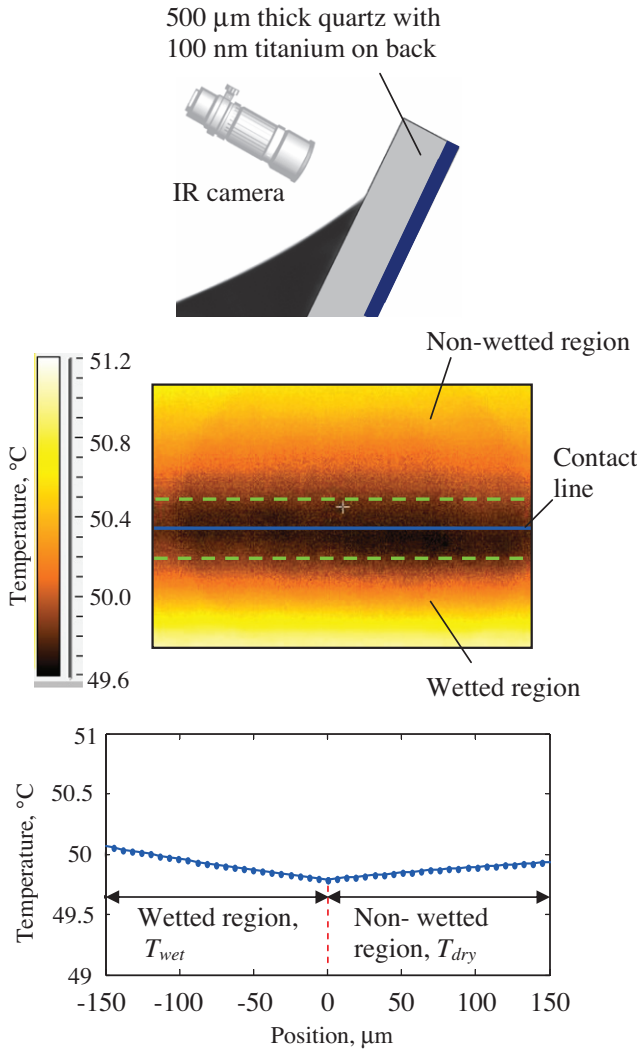


**Fig. 4.** IR image of quartz substrate under the heptane meniscus ( $q''_{net} = 600 \text{ W/m}^2$ ,  $\psi = 6.82 \times 10^{-7} \text{ kg/s}$ ). Dashed lines on the IR image delineate a region  $150 \mu\text{m}$  on either side of the contact line over which the analysis is conducted.

in temperature profile predicted numerically in [4] and measured experimentally in [13,16]. Larger temperature dips on the order of 1 K were measured by Sodtke et al. [15] and Dhavaleswarapu et al. [18]. The temperature dip measured in Ref. [15] was under a single FC-72 vapor bubble in nucleate boiling, while that in Ref. [18] was measured under a heptane meniscus that was constrained in a  $500 \mu\text{m}$ -wide channel. The channel constraint forced the meniscus profile to be very thin – at a distance of  $50 \mu\text{m}$  from the contact line, the meniscus thickness measured in Ref. [18] was  $\sim 50\%$  less than the thickness observed in this work, which could explain the differences in the temperature suppression.

### 3.3. Sub-region heat transfer

Assuming the evaporation rate from the meniscus to be constant at any location along the entire axial length of the groove, a heat balance analysis is carried out to estimate the heat dissipation through a small region of liquid near the contact line. This analysis neglects groove edge effects and the meniscus disturbance near the liquid feeder, as well as heat spreading within the substrate. The heat transfer rate from a liquid sub-region of length  $50 \mu\text{m}$  (thickness  $\sim 20 \mu\text{m}$ ) is examined.

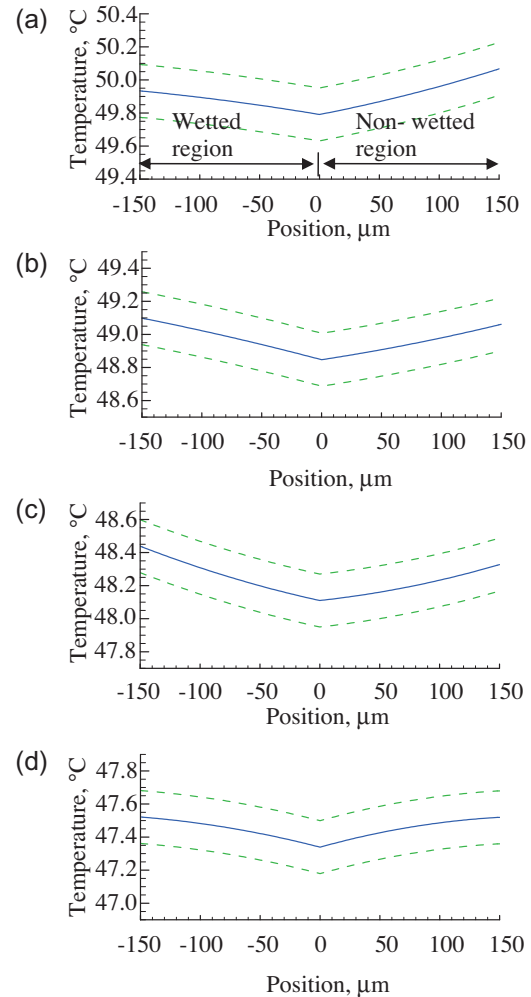


**Fig. 5.** IR temperature profiles of the groove wall top at  $y = 10 \text{ mm}$ ,  $q''_{net} = 600 \text{ W/m}^2$ , and different feeding rates: (a)  $6.01 \times 10^{-7} \text{ kg/s}$ , (b)  $6.55 \times 10^{-7} \text{ kg/s}$ , (c)  $6.82 \times 10^{-7} \text{ kg/s}$ , (d)  $7.10 \times 10^{-7} \text{ kg/s}$ .

On a per unit axial length of the groove basis, the heat balance for the control volume shown in Fig. 7 is given by

$$q'_{x_0} + q'_{x_0-\Delta x} + q'_{net} = q'_{sub-region} \quad (1)$$

where  $q'_{sub-region}$  is the heat dissipated per unit groove length by evaporation from the thin liquid film directly covering the top face of the control volume,  $q'_{net}$  is equal to the difference between  $q_{applied}$  and  $q_{loss}$  on a per unit length basis, and  $q'_{x_0}$  and  $q'_{x_0-\Delta x}$  represent the heat per unit length entering the control volume through the wall cross section just under the contact line ( $x_0$ ) and  $\Delta x$  from the contact line, respectively.  $q'_{net}$  is an order of magnitude smaller than  $q'_{x_0}$  and  $q'_{x_0-\Delta x}$ , and thus small variations in  $q'_{net}$  have little effect on  $q'_{sub-region}$ .

Temperature profiles such as those shown in Figs. 5 and 6 are divided into two portions,  $T_{wet}$  and  $T_{dry}$ , representing the groove wall temperature profiles in the wetted and non-wetted regions, respectively. A polynomial fit is applied to each profile (uncertainty  $\pm 0.03 \text{ K}$ ), thus allowing derivatives to be evaluated. Assuming 1D conduction, Eq. (1) yields

$$-k\delta \left. \frac{dT_{wet}}{dx} \right|_{x_0-\Delta x} + k\delta \left. \frac{dT_{dry}}{dx} \right|_{x_0} + q''_{net} \Delta x = q'_{sub-region} \quad (2)$$

where  $\Delta x$  is the length of the control volume, and  $k$ ,  $\delta$  are the thermal conductivity and thickness, respectively.

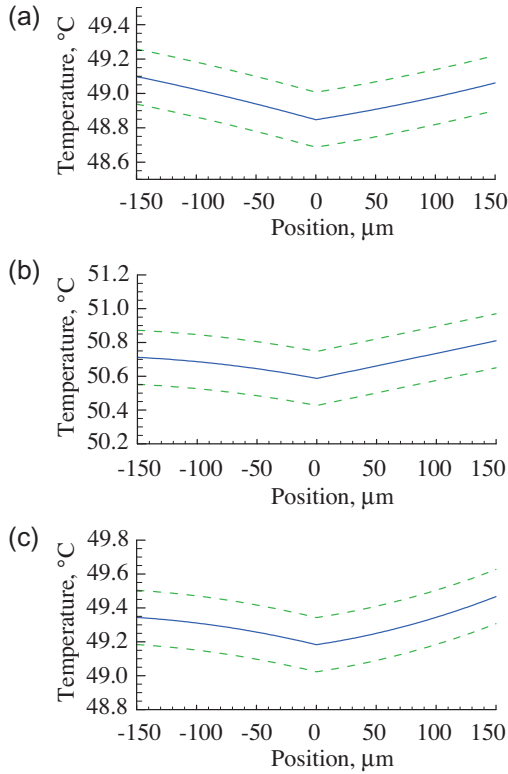


Fig. 6. IR temperature profiles of the groove wall top at feeding rate  $\psi = 6.55 \times 10^{-7}$  kg/s,  $q''_{net} = 600$  W/m<sup>2</sup>, and different measurement locations: (a)  $y = 10$  mm, (b)  $y = 20$  mm, (c)  $y = 30$  mm.

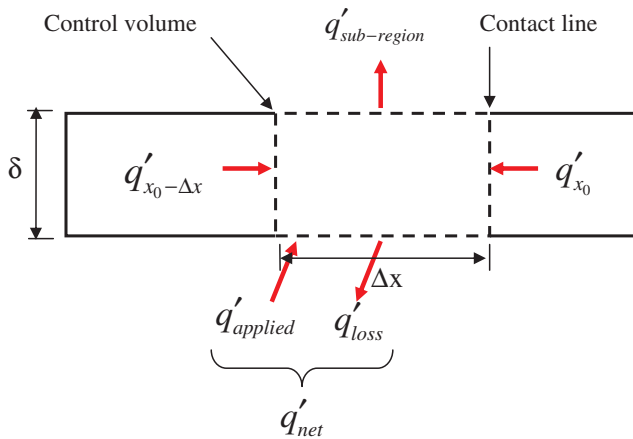


Fig. 7. Heat balance over the control volume in the groove substrate. The wall has a unit depth into page.

Table 1

Variation of sub-region percentage contribution ( $\eta$ ) to overall meniscus heat transfer with feeding rate ( $\psi$ ) and measurement location ( $y$ ).

$\psi$ (kg/s)	$y$		
	10 mm	20 mm	30 mm
$6.01 \times 10^{-7}$	47	45	54
$6.55 \times 10^{-7}$	48	41	49
$6.82 \times 10^{-7}$	40	47	46
$7.10 \times 10^{-7}$	46	39	41

To compare the thin-film region heat transfer relative to that from the entire meniscus, the fraction of heat being dissipated through a sub-region  $50 \mu\text{m}$  in length can be found by setting  $\Delta x = 50 \mu\text{m}$  in Eq. (2) and dividing  $q'_{sub-region}$  by the heat transfer per unit axial length dissipated by the meniscus

$$\eta = \frac{q'_{sub-region}}{\psi h_{fg} / W} \quad (3)$$

where  $\psi h_{fg}$  represents the total evaporative heat transfer from the meniscus and  $W$  is the axial length of the groove wall. Table 1 presents the percentage contribution of a  $50 \mu\text{m}$  sub-region to the overall meniscus heat transfer for the conditions explored.

It is seen in Table 1 that  $\eta$  is roughly the same for all cases, regardless of feeding rate or axial position along the groove.  $q'_{sub-region}$  was found to have an average value of  $2.14$  W/m with a standard deviation of  $0.14$  W/m. As will be shown in the next section, no trend with regard to axial measurement location or liquid feeding flowrate can be distinguished to within the measurement uncertainty. It may be concluded that since the meniscus profiles in the evaporating thin film region of the extended meniscus remain virtually the same throughout the range of tested feeding rates, the amount of heat transfer that is dissipated through the  $50 \mu\text{m}$  sub-region is relatively constant at  $\sim 45\%$  of the total. This result differs from the trend observed in Ref. [18] because in that experiment, the geometric constraint imposed by the channel forced the thickness of the meniscus to fall as the evaporation rate was increased, thus resulting in a lower thermal resistance and a higher fraction of the total heat transfer leaving through the sub-region.

### 3.4. Uncertainty analysis

Using the measurement uncertainties provided in the preceding sections, the uncertainty in the calculated quantities is determined using a standard propagation of uncertainty analysis

$$\sigma_f = \pm \sqrt{\sum_{i=1}^n (\theta_i \sigma_i)^2} \quad (4)$$

in which  $\sigma$  represents uncertainty in a particular parameter and  $\theta_i$  is the partial derivative of the function  $f$  with respect to each

Table 2  
Summary of uncertainty in calculated quantities.

Parameter	Uncertainty basis	Uncertainty value	Symbol in Eq. (5)
$q''_{net}$	Propagation of uncertainty in $q''_{applied}$ and $q''_{loss}$	$\pm 32.1$ W/m <sup>2</sup> (5.3%)	$\sigma_{q''_{net}}$
$\frac{dT_{dy}}{dx}  _{x_0}, t$	Standard deviation of $\frac{dT_{dy}}{dx}  _{x_0}$ over 0.17 s (10 frames)	$\pm 9.51 \times 10^{-4}$ K/ $\mu\text{m}^a$	$\sigma_{\frac{dT_{dy}}{dx}  _{x_0}, t}$
$\frac{dT_{dy}}{dx}  _{x_0}, y$	Standard deviation of $\frac{dT_{dy}}{dx}  _{x_0}$ over a 5 pixel band	$\pm 8.81 \times 10^{-4}$ K/ $\mu\text{m}^a$	$\sigma_{\frac{dT_{dy}}{dx}  _{x_0}, y}$
$\frac{dT_{wet}}{dx}  _{x_0 - \Delta x}, t$	Standard deviation of $\frac{dT_{wet}}{dx}  _{x_0 - \Delta x}$ over 0.17 s (10 frames)	$\pm 3.28 \times 10^{-4}$ K/ $\mu\text{m}^a$	$\sigma_{\frac{dT_{wet}}{dx}  _{x_0 - \Delta x}, t}$
$\frac{dT_{wet}}{dx}  _{x_0 - \Delta x}, y$	Standard deviation of $\frac{dT_{wet}}{dx}  _{x_0 - \Delta x}$ over a 5 pixel band	$\pm 3.58 \times 10^{-4}$ K/ $\mu\text{m}^a$	$\sigma_{\frac{dT_{wet}}{dx}  _{x_0 - \Delta x}, y}$
$\eta$	Propagation of uncertainty in $q''_{net}$ , $\psi$ , $\frac{dT_{dy}}{dx}  _{x_0}$ , $\frac{dT_{wet}}{dx}  _{x_0 - \Delta x}$	$\pm 0.23^a$	$\sigma_\eta$

<sup>a</sup> Corresponds to  $\psi = 6.01 \times 10^{-7}$  kg/s at  $y = 10$  mm case.

independent quantity. The sub-region contribution,  $\eta$ , is dependent on the temperature derivatives  $\frac{dT_{wet}}{dx}|_{x_0-\Delta x}$  and  $\frac{dT_{dry}}{dx}|_{x_0}$ . The uncertainties of these quantities with respect to time and position are taken as the standard deviation of the evaluated derivative terms over 10 image frames and a 5 pixel band (in the axial direction,  $y$ ), respectively. Averaging temperatures over a 20 pixel band yielded only a minor change of order 0.01 K from the 5 pixel band case.  $\eta$  is also dependent on the net applied heat flux,  $q''_{net}$ , and the liquid feeding rate,  $\psi$ . Application of Eq. (4) gives the following uncertainty in  $\eta$ :

$$\sigma_{\eta} = \sqrt{\left(\frac{\Delta x}{\psi h_{fg}/W} \sigma_{q''_{net}}\right)^2 + \left(\frac{-k\delta}{\psi h_{fg}/W}\right)^2 \left[\sigma_{\frac{dT_{wet}}{dx}|_{x_0-\Delta x},t}^2 + \sigma_{\frac{dT_{wet}}{dx}|_{x_0-\Delta x},y}^2\right] + \left(\frac{k\delta}{\psi h_{fg}/W}\right)^2 \left[\sigma_{\frac{dT_{dry}}{dx}|_{x_0},t}^2 + \sigma_{\frac{dT_{dry}}{dx}|_{x_0},y}^2\right] + \left(\frac{q'_{sub-region}}{\psi^2 h_{fg}/W} \sigma_{\psi}\right)^2} \quad (5)$$

Taking representative values corresponding to the  $\psi = 6.01 \times 10^{-7}$  kg/s,  $y = 10$  mm case (given in Table 2), and with  $W = 50$  mm,  $\Delta x = 50$   $\mu$ m,  $h_{fg} = 350.6$  kJ/kg, and  $q'_{sub-region} = 2.0$  W/m, the uncertainty in  $\eta$  is  $\sigma_{\eta} = \sqrt{1.45 \times 10^{-7} + 5.96 \times 10^{-3} + 4.25 \times 10^{-2} + 3.32 \times 10^{-3}} = \pm 0.23$ . This corresponds to an uncertainty of nearly  $\pm 50\%$  in the calculated value of  $\eta$ . The largest contributions to uncertainty in  $\eta$  come from the temperature derivative terms due to the measurement noise. While averaging temperature profiles over time and position helps to reduce the uncertainty, the underlying uncertainty in the temperature measurements themselves must be reduced to improve analysis accuracy.

#### 4. Conclusions

An evaporating liquid meniscus in a horizontal V-groove that was open to the atmosphere has been investigated to determine the contribution of the evaporating thin film region to the heat transfer in this geometry. Microscale infrared thermography was used to obtain high-resolution temperature profiles of the groove wall at three axial locations. A temperature suppression of  $\sim 0.2$  K was observed at the contact line relative to the temperature at a location 150  $\mu$ m on each side of the contact line. It was found that in the setup used, a sub-region 50  $\mu$ m in length accounts for up to  $\sim 45\%$  of the meniscus heat transfer at a given axial location through a range of liquid feeding rates. Noise in the temperature measurements leads to an uncertainty of nearly  $\pm 50\%$  in the estimated sub-region heat transfer. As a result, trends in sub-region heat transfer with respect to changes in liquid feeding rate and axial position along the groove are inconclusive; however, the importance of the evaporating thin film region to total meniscus heat transfer is clearly established.

#### Acknowledgement

The authors acknowledge financial support for this work from the Cooling Technologies Research Center, a National Science

Foundation Industry/University Cooperative Research Center at Purdue University.

#### References

- [1] B.V. Deryagin, Definition and the concept of, and magnitude of the disjoining pressure and its role in the statics and kinetics of thin layers of liquids, *Colloid J. USSR* 17 (1955) 191–197.
- [2] M. Potash Jr., P.C. Wayner Jr., Evaporation from a two-dimensional extended meniscus, *Int. J. Heat Mass Transfer* 15 (10) (1972) 1851–1863.
- [3] P.C. Wayner Jr., Intermolecular forces in phase-change heat transfer: 1998 Kern award review, *AIChE J.* 45 (10) (1999) 2055–2068.
- [4] S.S. Panchangam, A. Chatterjee, J.L. Plawsky, P.C. Wayner Jr., Comprehensive experimental and theoretical study of fluid flow and heat transfer in a microscopic evaporating meniscus in a miniature heat exchanger, *Int. J. Heat Mass Transfer* 51 (21–22) (2008) 5368–5379.
- [5] F.W. Holm, S.P. Goplen, Heat transfer in the meniscus thin-film transition region, *J. Heat Transfer* 101 (3) (1979) 543–547.
- [6] X. Xu, V.P. Carey, Film evaporation from a micro-grooved surface – an approximate heat transfer model and its comparison with experimental data, *J. Thermophys. Heat Transfer* 4 (4) (1990) 512–520.
- [7] P.C. Stephan, C.A. Busse, Analysis of the heat transfer coefficient of grooved heat pipe evaporator walls, *Int. J. Heat Mass Transfer* 35 (2) (1992) 383–391.
- [8] H.B. Ma, G.P. Peterson, Experimental investigation of the maximum heat transport in triangular grooves, *J. Heat Transfer* 118 (3) (1996) 740–746.
- [9] H.K. Dhavaleswarapu, P. Chamarthy, S.V. Garimella, J.Y. Murthy, Experimental investigation of steady buoyant-thermocapillary convection near an evaporating meniscus, *Phys. Fluids* 19 (8) (2007) 082103.
- [10] P. Chamarthy, H.K. Dhavaleswarapu, S.V. Garimella, J.Y. Murthy, S.T. Wereley, Visualization of convection patterns near an evaporating meniscus using  $\mu$ PIV, *Exp. Fluids* 44 (3) (2008) 431–438.
- [11] R.D. Deegan, O. Bakajin, T.F. Dupont, G. Huber, S.R. Nagel, T.A. Witten, Capillary flow as the cause of ring stains from dried liquid drops, *Nature* 389 (6653) (1997) 827–829.
- [12] H.K. Dhavaleswarapu, C.P. Migliaccio, S.V. Garimella, J.Y. Murthy, Experimental investigation of evaporation from low-contact-angle sessile droplets, *Langmuir* 26 (2) (2010) 880–888.
- [13] C. Höhmann, P. Stephan, Microscale temperature measurement at an evaporating liquid meniscus, *Exp. Therm. Fluid Sci.* 26 (2–4) (2002) 157–162.
- [14] C. Buffone, K. Sefiane, Temperature measurement near the triple line during phase change using thermochromic liquid crystal thermography, *Exp. Fluids* 39 (1) (2005) 99–110.
- [15] C. Sodtke, J. Kern, N. Schweizer, P. Stephan, High resolution measurements of wall temperature distribution underneath a single vapor bubble under low gravity conditions, *Int. J. Heat Mass Transfer* 49 (5–6) (2006) 1100–1106.
- [16] J. Jiang, Y.-X. Tao, L. Byrd, Evaporative heat transfer from thin liquid film on a heated cylinder, *Int. J. Heat Mass Transfer* 43 (1) (2000) 85–99.
- [17] C. Buffone, K. Sefiane, IR measurements of interfacial temperature during phase change in a confined environment, *Exp. Therm. Fluid Sci.* 29 (1) (2004) 65–74.
- [18] H.K. Dhavaleswarapu, S.V. Garimella, J.Y. Murthy, Microscale temperature measurements near the triple line of an evaporating thin liquid film, *J. Heat Transfer* 131 (6) (2009) 061501 (7pp.).
- [19] Paints, NASA Jet Propulsion Laboratory. <<http://masterweb.jpl.nasa.gov/reference/paints.htm>>.
- [20] MATLAB, The Language of Technical Computing, version 7.6, The Mathworks Inc., Natick, MA, 2008.